Spatially resolved absolute diffuse reflectance measurements for noninvasive determination of the optical scattering and absorption coefficients of biological tissue

Alwin Kienle, Lothar Lilge, Michael S. Patterson, Raimund Hibst, Rudolf Steiner, and Brian C. Wilson

The absorption and transport scattering coefficients of biological tissues determine the radial dependence of the diffuse reflectance that is due to a point source. A system is described for making remote measurements of spatially resolved absolute diffuse reflectance and hence noninvasive, noncontact estimates of the tissue optical properties. The system incorporated a laser source and a CCD camera. Deflection of the incident beam into the camera allowed characterization of the source for absolute reflectance measurements. It is shown that an often used solution of the diffusion equation cannot be applied for these measurements. Instead, a neural network, trained on the results of Monte Carlo simulations, was used to estimate the absorption and scattering coefficients from the reflectance data. Tests on tissue-simulating phantoms with transport scattering coefficients between 0.5 and 2.0 mm^{-1} and absorption coefficients between 0.002 and 0.1 mm^{-1} showed the rms errors of this technique to be 2.6% for the transport scattering coefficient and 14% for the absorption coefficients. The optical properties of bovine muscle, adipose, and liver tissue, as well as chicken muscle (breast), were also measured *ex vivo* at 633 and 751 nm. For muscle tissue it was found that the Monte Carlo simulation did not agree with experimental measurements of reflectance at distances less than 2 mm from the incident beam.

Key words: Tissue optics, reflectance, Monte Carlo, neural network.

1. Introduction

Understanding the propagation and the distribution of light in biological tissue is essential for effective and safe applications in medical diagnostics and therapeutics.[1,2] Light propagation in biological tissue, which is an optically turbid (i.e., scattering and absorbing) medium, can be described by the Boltzmann transport equation.[3] This involves three optical properties: the absorption coefficient μ_a, the scattering coefficient μ_s, and the scattering phase function. In the diffusion approximation[3] to the Boltzmann equation, the phase function is represented by the mean cosine of the scattering angle g, which is combined with the scattering coefficient to give the reduced (or transport) scattering coefficient $\mu_s' = \mu_s(1 - g)$.

The various methods of measuring the optical properties of tissues have been recently reviewed by Wilson[4] and Cheong *et al.*[5] Substantial discrepancies are evident in the published data, which may be attributed, at least in part, to the different experimental methods employed and the theoretical models used to analyze the measurements. A number of these methods are invasive, requiring excised tissue specimens.[6,7] Minimally invasive or noninvasive techniques include interstitial measurements with

A. Kienle, R. Hibst, and R. Steiner are with the Institut für Lasertechnologien in der Medizin, Ulm, Germany; L. Lilge and M. Patterson are with the Hamilton Regional Cancer Centre and McMaster University, Hamilton, Ontario, Canada; B. C. Wilson is with the Ontario Laser and Lightwave Research Centre, Toronto, Ontario, Canada. L. Lilge and B. C. Wilson are also with the Ontario Cancer Institute/Princess Margaret Hospital and Department of Medical Biophysics, University of Toronto, Toronto, Ontario, Canada.

Received 16 March 1995; revised manuscript received 7 August 1995.

0003-6935/96/132304-11$10.00/0

isotropic detectors,[8] time-domain[9] and frequency-domain[10] measurements of (laser) light reflectance or transmittance, or coherent backscattering.[11]

Steady-state spatially resolved measurement of diffuse reflectance from a point source or narrow collimated beam has also been investigated[12] by the use of multiple fiber-optic detectors in contact with the tissue surface at varying distances from the source. This has the advantage of requiring relatively simple technology compared with that of the time-dependent techniques. However, measurements are made at only a limited number of points (typically 6–8) so that the estimates of the derived optical properties may be biased by local tissue inhomogeneities. Pressure that is due to the contact probe may also affect the optical properties derived, for example, because of altered local blood content. Recently Bolt and ten Bosch[13,14] introduced an alternative diffuse reflectance technique (video reflectometry) based on a remote, noncontact, video camera detector, which potentially may overcome these limitations. Jacques *et al.*[15] used this method for measurements on *ex vivo* tissue. Results obtained with similar systems have also been reported by Splinter *et al.*[16] and by Dogariu and Asakura.[17]

In either the remote or the contact diffuse reflectance techniques, a model of light transport in tissue is required for relating the diffuse reflectance values to the optical absorption and reduced scattering coefficients of the tissue in order to extract these coefficients. This is usually done in an iterative fashion by using the model to fit the measured data, with the optical properties as free parameters. Various authors have used solutions of the diffusion equation for this purpose.[12] Because diffusion theory restricts the degree of anisotropy in the radiance within the tissue, a particular problem arises in handling the boundary conditions at the tissue surface, where the radiance pattern is changing rapidly. Different models of varying degrees of sophistication have been developed to describe these boundary conditions. A primary objective of the present work was to investigate the accuracy of these analytic models, by the use of both simulated reflectance data generated by a Monte Carlo code and experimental measurements made in optical phantoms and tissues with a video reflectometry system similar to that of Jacques *et al.*[15]

In those cases in which an analytic model does not accurately represent the reflectance, more exact models of light propagation may be applicable. The alternative approaches of using either higher-order analytic solutions to the Boltzmann equation or using Monte Carlo simulation of photon paths are generally too complex or computationally expensive to be used in iterative fitting of reflectance data.[8] In an earlier paper[19] we have demonstrated the use of a neural network trained with data generated by a diffusion model to derive the optical scattering and absorption properties from spatially resolved diffuse reflectance measurements. Such networks may also be trained by the use of either Monte Carlo simulated data or experimental phantom data generated over the range of optical properties of interest. This approach does not rely on any approximate model of radiation transport, and, once the network is trained, it is computationally fast.

In the work of Farrell *et al.*,[19] the neural network was applied to a contact-probe instrument, and, because of the possible variation in the optical coupling between the fibers and the tissue, only the relative shape of the reflectance versus the distance curve was used, not the absolute values of local reflectance. Furthermore, there are limitations on the shortest radial distance at which measurements can be made with a fiber-optic probe. Potential advantages of video reflectometry are that absolute measurements are possible and that the full range of distances on the surface can be used.

To assess this potential, we have made spatially resolved absolute diffuse reflectance measurements at two different wavelengths in tissue-simulating phantoms of known optical properties by using a CCD camera video reflectometer. We found that diffusion theory[12] did not provide an accurate prediction of the absolute local reflectance calculated by Monte Carlo simulations, and its application gave poor estimates of the optical properties. Therefore a Monte Carlo trained neural network was used to analyze the results. Experimental measurements of representative mammalian soft tissues *ex vivo* were also made for comparison with published values. For tissues, we found that even Monte Carlo simulations did not always provide a good description of the reflectance close to the source. When absolute reflectance data for 2–12-mm distances are used in the neural network, we estimate that the transport scattering coefficient can be determined with 3%–4% accuracy and the absorption coefficient can be determined with 10–15% accuracy.

2. Theory and Modeling

In this section we describe the two models of radiation transport that were used to derive the absorption and scattering coefficients from the spatially resolved measurements of diffuse reflectance. The first was a Monte Carlo simulation of photon transport that involves no physical approximations but that produces estimates of the reflectance subject to statistical uncertainties. Reducing these uncertainties to acceptable values, especially for locations far from the source, requires that many photon histories be traced. The time required for this precludes the use of iterative Monte Carlo simulations, so, as described below, results of many simulations were used to train a neural network to derive μ_a and μ_s' from experimental data. An alternative approach is to use an approximate transport model to generate an analytic expression for the spatially resolved reflectance. Physical approximations must be made, but results can be generated quickly, so that conven-

tional least-squares techniques can be used to generate best estimates of μ_a and μ_s'. We used a diffusion model to generate analytical expressions for the reflectance.

The principles of Monte Carlo simulation of particle transport have been thoroughly described,[20,21] so we point out only the salient features of our simulations. The tissue was assumed to be a semi-infinite half-space with scattering coefficient μ_s, absorption coefficient μ_a, and index of refraction n, which was $n = 1.4$ for the simulations.[22] The scattering phase function was that originally used by Henyey and Greenstein[23] in which the angular dependence is described by one parameter, g. All photons were assumed to be normally incident at the origin; the influence of the actual incident-beam shape was incorporated by convolution, as described below. Specular reflection at the tissue–air boundary was handled with the assumption that the usual Fresnel equations could be used to calculate the fraction of photon weight transmitted and reflected.

Because we wish to calculate the absolute signal received by the detector, it is necessary to estimate the fraction of diffusely reflected photons that enters the aperture of the detector. This can be done in two ways. One is to track the direction of photons that are emitted from the tissue surface and to score only those that intercept the detector aperture. Because most photons will not be detected, this is inefficient. We accelerated the Monte Carlo simulations with a variance-reduction method called last flight estimation.[7,24] In this method, at each interaction point the probability that the photon will escape the medium without further interaction and intercept the detector is calculated. This variance-reduction method is valid if the solid angle of detection is small (i.e., the detector size is much smaller than the distance from the detector to the sample, as is the case in our experiment). An alternative approach is to score all photons that are emitted from a surface element but to assume that the reflectance is Lambertian so that all directions are equally probable. The detected signal is then derived from the solid angle subtended by the aperture. Because all emitted photons contribute to the calculated signal, this method is computationally efficient, and its validity was tested by a comparison of calculations made with both techniques.

Another way to improve the efficiency of Monte Carlo calculations is to employ the principle of similarity. It has long been known that different combinations of g and μ_s will yield similar results for dependent quantities, such as the diffuse reflectance.[25] The simplest relationship, which is incorporated in diffusion theory, is that conservation of the quantity $(1 - g)\mu_s$ will ensure similarity. We tested this relationship to determine whether Monte Carlo simulations performed with one value of the anisotropy parameter g were sufficient to derive μ_a and μ_s' for materials with a range of μ_s and g.

Two neural networks were set up to solve the inverse problems. One (NN1) consisted of 11 input nodes, representing the reflectance at 11 distances, and 11 hidden nodes linked to two output nodes. The other (NN2) had 9 input and hidden nodes with two output nodes. In principle these output nodes could represent μ_a and μ_s' directly, but we followed the alternative approach described in detail by Farrell *et al.*[19] Instead of training the network with the reflectance as a function of distance $R(\rho)$, the function $\log_e[\rho^2 R(\rho)]$ was used. This function has two distinctive features: a peak a few millimeters from the source and a roughly exponential decrease far from the source. The position of the peak depends strongly on $\mu_t' = \mu_s' + \mu_a$, and the slope of the exponential part depends on the effective attenuation coefficient μ_{eff}. In the diffusion approximation, $\mu_{\text{eff}} = [3\mu_a(\mu_a + \mu_s')]^{1/2}$. The neural networks were trained with μ_t' and μ_{eff} as the output nodes, as these are the recognizable features of the $\log_e[\rho^2 R(\rho)]$ versus ρ curve. The coefficients μ_a and μ_s' were then calculated from these values. NN1 was trained with the reflectance data at $\rho = 2, 3, 4, \ldots, 12$ mm, and NN2 was trained with the data at $\rho = 2, 2.5, 3, \ldots, 6$ mm. The use of two networks accommodates the wide range of attenuation encountered in real tissues. 120 Monte Carlo simulations were performed that covered the range of $0.2 < \mu_s' < 2.5$ mm^{-1} and $0.001 < \mu_a < 0.5$ mm^{-1}. The number of photons N used in each Monte Carlo simulation was calculated from the empirical formula

$$N = [(\mu_a/\mu_s')^{1/2}]^{1/2} \times 10^6$$

in order to give comparable statistics over the required distance range. The radial bin in the Monte Carlo simulations was 40 μm. If the ratio of reflectance at 12 mm to the reflectance at the origin was greater than 3×10^{-5}, the data from that simulation were used to train NN1; if the ratio was less than 2×10^{-4}, the data formed part of the training set for NN2 (note that a few simulations were used to train both networks). After training, the rms error in μ_{eff} and μ_t' were 4.6% for NN1 and 3.5% for NN2. Assuming that the errors in μ_t' and μ_{eff} are uncorrelated, the expected errors in μ_a and μ_s' would be approximately 8% and 5%, respectively, for NN1 and approximately 6% and 4% for NN2. The reasons for using data only for distances greater than 2 mm are discussed below.

The diffusion model used to generate an analytic expression for the reflectance has been described by Farrell *et al.*[12] The final result is

$$R(\rho) = \frac{a'}{4\pi}\left[\frac{1}{\mu_t'}\left(\mu_{\text{eff}} + \frac{1}{r_1}\right)\frac{\exp(-\mu_{\text{eff}} r_1)}{{r_1}^2} + \left(\frac{1}{\mu_t'} + 2z_b\right)\left(\mu_{\text{eff}} + \frac{1}{r_2}\right)\frac{\exp(-\mu_{\text{eff}} r_2)}{{r_2}^2}\right], \quad (1)$$

where

$$r_1 = \left[\left(\frac{1}{\mu_t'}\right)^2 + \rho^2\right]^{1/2},$$

$$r_2 = \left[\left(\frac{1}{\mu_t'} + 2z_b\right)^2 + \rho^2\right]^{1/2},$$

$$a' = \mu_s'/(\mu_a + \mu_s'),$$

and z_b is the distance from the tissue surface to an extrapolated boundary at which the fluence rate is forced to be 0. In deriving Eq. (1) it was assumed that all incident photons are isotropically scattered at a depth $1/\mu_t'$. As described by Farrell *et al.*,[12] calculations were also performed with an extended source,

$$S(z) = a'\mu_t' \exp(-\mu_t' z), \tag{2}$$

where the initial scatter events are exponentially distributed along the z axis. A cylindrically symmetric three-dimensional source function was also applied:

$$S(\rho, z) = \frac{9a'\mu_t^3}{2\pi} \exp[-\mu_t(z + 3\rho)]. \tag{3}$$

We used a three-dimensional convolution to calculate the spatially resolved reflectance from Eq. (3).

3. Materials and Methods

Figure 1 shows a schematic of the experimental setup for spatially resolved absolute diffuse reflectance measurements. A He–Ne laser (Spectra Physics, Mountain View, Calif.) emitting at 633 nm (beam diameter 0.4 mm) or a 751-nm laser diode (Oriel, Stamford, Conn.) served as light sources. The laser beam was deflected onto the specimen by a mirror at an angle of incidence of 5° to 10° to avoid the detection of specularly reflected light. (We confirmed by Monte Carlo simulation that this small angle did not cause a significant difference in the spatially resolved reflectance.) The diffusely reflected light was detected by a CCD camera (Photometrics, Tucson, Ariz.) mounted coaxially with the normal to the specimen surface. The sample was viewed through a 2.62-mm aperture in front of an imaging objective (f = 50 mm; Nikon, Japan). The purpose of the aperture was to define the acceptance angle of the detector for the calculation of absolute reflectance. The distance between the aperture and the sample was fixed at 110 mm, and a 4 cm × 4 cm area was imaged onto the 1024 × 1024 pixels of the CCD. The CCD was equipped with a 14-bit analog-to-digital converter, giving a dynamic range of approximately 10^4. Total incident power in the 1–100-μW range was sufficient for these experiments in which the image acquisition time was 1 s. Neutral-density filters were used to adjust the incident laser power to avoid saturation of the detector system. Control of the CCD readout, data processing, and storage was executed by a PC. For data reduction and analysis, the radial distance of each pixel to the center of the laser beam was calculated and the pixel values were sorted into bins that correspond to a radial width of 40 μm at the sample. In some experiments, linear polarizers in the light delivery and detection paths were used to investigate the influence of the polarization state on diffuse reflectance.

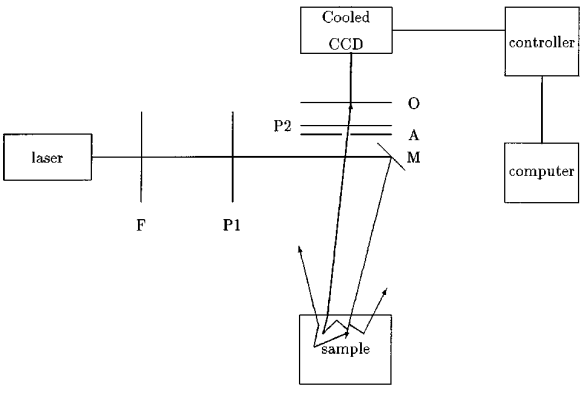

Fig. 1. Experimental arrangement for the measurement of spatially resolved absolute diffuse reflectance. Components are M, mirror; F, neutral-density filter; P1, P2, linear polarizers; O, camera lens; A, aperture. For characterization of the incident laser beam, a second mirror was used to reflect the beam into the detector aperture.

The accuracy and the limitations of the system were tested in tissue-simulating phantoms that comprised Intralipid (Liposyn, 20% stock solution; Abbott Lab., Montreal, Quebec), a lipid emulsion that provided light scattering, and Trypan Blue dye (Sigma, East St. Louis, Ill.) as the absorber. The reduced scattering coefficient of Intralipid was measured by an established frequency-domain diffuse reflectance technique[26] as $\mu_s' = 1.40 \pm 0.05$ mm^{-1} for a 1% volume concentration at 633 nm. The scattering coefficient μ_s was determined with collimated transmission measurements to be $\mu_s = 7.1$ mm^{-1}.[18] Thus for the anisotropy factor we used $g = 0.8$. The absorption coefficient of Intralipid was determined with the video reflectometry apparatus described in this paper to be $\mu_a = 0.0005$ mm^{-1}. This compares well with $\mu_a = 0.0006$ mm^{-1} measured by Fishkin *et al.*[27] The absorption coefficient of trypan blue was determined by a conventional spectrophotometer for each solution. The total volume of the phantom was 400 mL (7.5 cm × 7.5 cm × 7.0 cm), and boundary effects were not significant.

Careful characterization of the laser beam is essential, as this method is based on absolute values of the spatially resolved reflectance. We measured the laser beam by replacing the turbid phantom with a mirror and directing the beam into the camera aperture. Reflectance losses by this second mirror have to be considered and were measured separately. A Gaussian profile was fitted to the measured laser beam and convolved with the pencil-beam reflectance calculated by the models described in Section

2. The total power in the laser beam was also measured by an optical power meter (Newport, Irvine, Calif.). This measurement was repeated before all sample measurements were taken so that correction could be made for drifts in source power.

Fresh tissue samples were obtained from a local butcher, stored at +4 °C, and used within 8 h for the *ex vivo* experiments. The samples had not been frozen nor were they treated to remove blood. Measurements were done after the samples had reached room temperature at locations where there were no obvious inhomogeneities.

The optical properties of bovine fat, muscle, and liver, and chicken breast were determined, and measurements were made at three to six different locations on each tissue sample. For bovine liver and chicken breast, the sample thickness was limited to ~20 mm but was greater than 40 mm for bovine muscle and fat. The tissue surface was aligned approximately horizontally.

4. Results

In this section we first present results concerning variance reduction and similarity in the Monte Carlo simulations. This is followed by a comparison of Monte Carlo simulations and diffusion-theory calculations together with a discussion of the errors incurred in using the diffusion model to estimate μ_a and μ_s'. Next, experimental measurements on tissue-simulating phantoms are presented as well as an assessment of the accuracy of the optical properties derived with the Monte Carlo–neural-network approach. Finally, we present data obtained for a range of animal tissue *ex vivo*.

Figure 2 shows calculations of the dependence of the diffuse reflectance on polar angle at three distances from the source for the case $\mu_s' = 1.0\ \text{mm}^{-1}$, $\mu_a = 0.01\ \text{mm}^{-1}$, and $g = 0.9$. Also shown is the perfectly diffuse or Lambertian distribution. In general, the angular distribution is more peaked toward small angles than the Lambertian distribution, and the difference is greatest at positions small distances from the source. Of more direct interest is Fig. 3, in which the diffuse reflectance through the detector aperture is plotted versus distance from the source. Here a direct comparison is made between calculations based on the true angular distribution of the remitted photons by the use of last flight estimation as a variance-reduction method and calculations based on a Lambertian distribution. Except for locations closer than 0.05 mm to the source, there is no significant difference in the curves. Because of the large increase in efficiency, all Monte Carlo results presented hereafter were obtained with the assumption of a Lambertian distribution.

The issue of similarity is addressed in Fig. 4. In Fig. 4(a) the spatially resolved reflectance is shown as a function of distance for three Monte Carlo simulations. For all three simulations, $(1 - g)\mu_s = 1.0\ \text{mm}^{-1}$ and $\mu_a = 0.01\ \text{mm}^{-1}$, but three values of g were used: 0, 0.8, and 0.95, and μ_s was adjusted accordingly. If the simple similarity relation were true, all three curves would be identical. This is clearly not the case for $g = 0$ compared with $g = 0.8$,

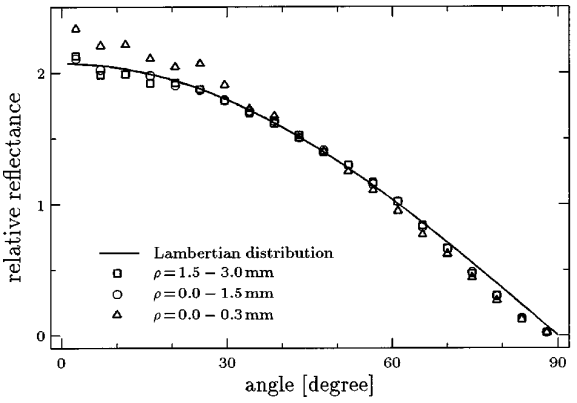

Fig. 2. Angular distribution of diffusely reflected light as calculated by Monte Carlo simulation for $\mu_s' = 1.0\ \text{mm}^{-1}$, $\mu_a = 0.01\ \text{mm}^{-1}$, $g = 0.9$, and an incident pencil beam. Results are shown for three radial bins: 0–1.5 mm, 1.5–3.0 mm, and 0–0.3 mm. The Lambertian distribution is also shown as a solid curve. Deviation from the Lambertian distribution is greatest for regions close to the source.

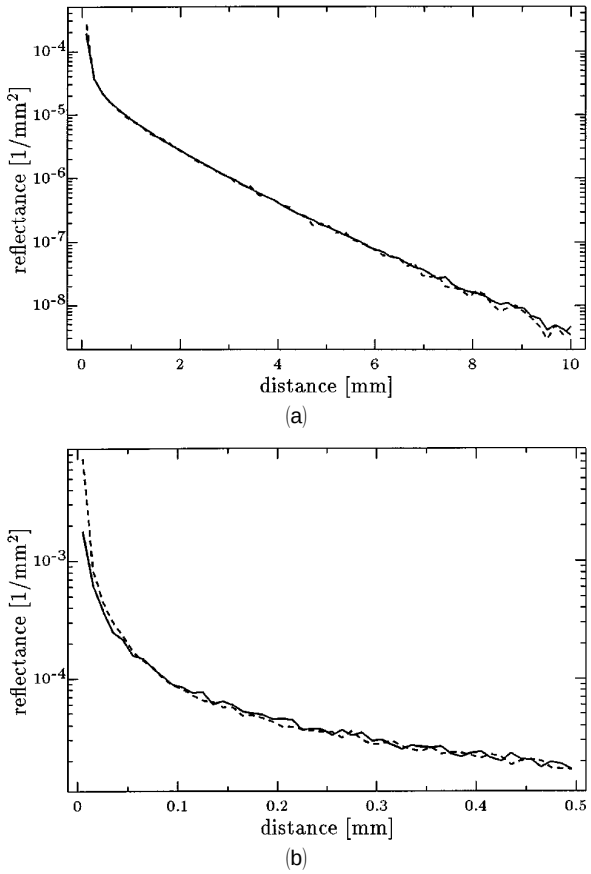

Fig. 3. Spatially resolved diffuse reflectance calculated by Monte Carlo simulations, assuming a Lambertian distribution of emitted light (solid curve) and explicit calculations based on the actual angular distribution (dashed curve). Conditions for the simulations are the same as those in Fig. 2. A pencil beam is used for the incident beam. As shown in (b), the only significant deviation occurs within 0.05 mm of the incident pencil beam.

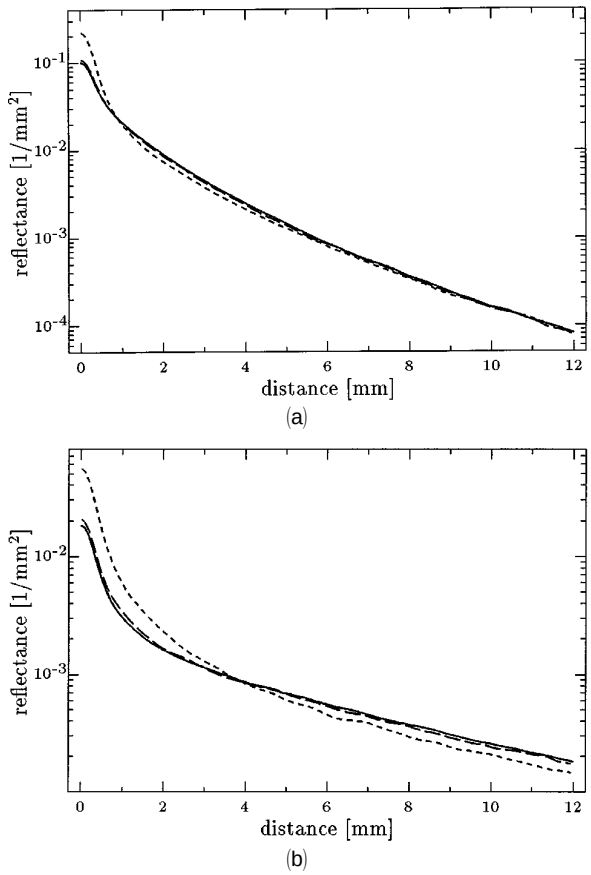

Fig. 4. Tests of the similarity relation that use Monte Carlo simulations for spatially resolved reflectance. For (a), $\mu_s' = 1.0$ mm^{-1}, $\mu_a = 0.01$ mm^{-1}, and $g = 0$ (short-dashed curve), 0.8 (long-dashed curve), 0.95 (solid curve). The incident beam was 0.4 mm in diameter. Conditions were the same for (b) except that $\mu_s' = 0.2$ mm^{-1}.

but the difference between the curves for $g = 0.8$ and $g = 0.95$ is at most 8%. This is similar even when μ_s' is reduced to 0.2 mm^{-1}. Although Monte Carlo simulations could be greatly accelerated by the use of an isotropic phase function ($g = 0$), this is not justified here. However, because the simple similarity relationship does appear to hold over the range $0.8 < g < 0.95$, which is typical of mammalian soft tissues in the visible and near infrared,[5] all the following Monte Carlo data were obtained for $g = 0.9$.

In Fig. 5 we compare the results of a Monte Carlo simulation for $\mu_s' = 1.0$ mm^{-1}, $\mu_a = 0.1$ mm^{-1}, and $g = 0.9$ with those obtained from Eq. (1). There are large differences even far from the source, although the diffusion curve eventually takes on the correct shape. Implementing the more complex one-dimensional and three-dimensional sources does little to improve the agreement with the Monte Carlo results. To assess the effect this disagreement would have on estimates of μ_a and μ_s' made with the diffusion model, the Monte Carlo results were treated as experimental data and μ_a and μ_s' were altered to generate the best fit of Eq. (1) to these data. The results are summarized in Table 1, for which the

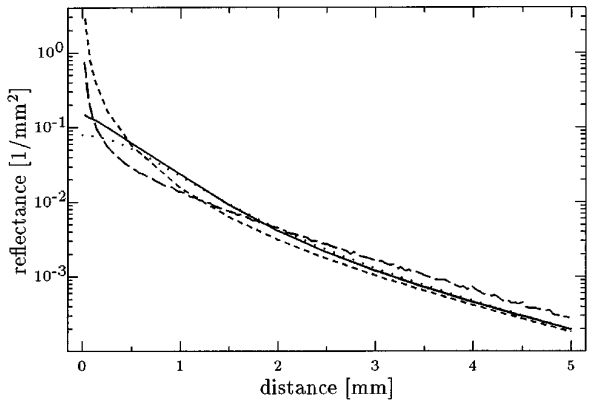

Fig. 5. Comparison of the spatially resolved diffuse reflectance estimated by Monte Carlo simulation (long-dashed curve) to diffusion-theory calculations for an incident pencil beam. Diffusion theory used a single scatter source (dotted curve), an extended one-dimensional source (short-dashed curve), or a three-dimensional source (solid curve). The optical properties were $\mu_s' = 1.0$ mm^{-1}, $\mu_a = 0.1$ mm^{-1}, and $g = 0.9$.

fitting has been performed over different distance ranges. When the full range (0–12.8 mm) was used, the estimates of μ_a and μ_s' were the most accurate but the fit to the experimental reflectance data was poorest. As the data closer to the source were excluded, the goodness of fit improved but the error in the fitted optical properties increased to greater than 50%. We conclude that the diffusion expression in Eq. (1) is inadequate for the analysis of absolute reflectance data.

In Table 2 we present the estimates of μ_a and μ_s' obtained by the Monte Carlo–neural network method for 13 tissue-simulating phantoms together with the true optical properties measured independently by the frequency-domain technique. In three solutions with different concentrations of Intralipid, different amounts of Trypan Blue were successively added to alter the absorption coefficient. In Fig. 6 we show the experimental reflectance data for five of the phantoms as well as Monte Carlo results generated with the known values of μ_a and μ_s' from Table 2. (Note that these simulations incorporate the measured shape of the incident beam.) The agreement is quite good for all cases over the full distance range. From Table 2 it is evident that the scattering coefficient is determined more accurately than

Table 1. Optical Properties Derived when Eq. (1) is Fit to Monte Carlo-Generated Data for $\mu_s' = 1.0$ mm^{-1}, $\mu_a = 0.01$ mm^{-1} and $g = 0.9$[a]

Fitted Values	Fitting Range (mm)				
	0–12.8	1–12.8	2–12.8	3–12.8	4–12.8
μ_s' (mm^{-1})	1.07	1.46	1.58	1.76	1.49
μ_a (mm^{-1})	0.0083	0.0049	0.0040	0.0026	0.0046
σ	0.218	0.118	0.087	0.104	0.093

[a] σ is the rms difference between the logarithm of the Monte Carlo data and the logarithm of diffuse reflectance calculated according to Eq. (1). As points close to the source are excluded, the fit is improved, but the error in μ_a and μ_s' is increased.

Table 2. Estimates of μ_a and μ_s' Obtained by Neural Networks for a Series of Tissue-Simulating Phantoms Compared with True Values Based on Independent Measurements[a]

True Optical Properties		Neural Network Results	
μ_a (mm^{-1})	μ_s' (mm^{-1})	μ_a (mm^{-1})	μ_s' (mm^{-1})
0.0022	1.99	0.0023	1.99
0.0057	1.98	0.0047	1.95
0.0143	1.97	0.0150	1.97
0.0033	0.98	0.0034	1.00
0.0088	0.98	0.0083	1.03
0.025	0.97	0.022	0.99
0.070	0.94	0.075*	0.95*
0.100	0.93	0.107*	0.96*
0.0022	0.50	0.0017	0.52
0.0065	0.50	0.0053	0.52
0.020	0.49	0.020	0.51
0.043	0.49	0.048*	0.49*
0.073	0.49	0.083*	0.48*

[a]Values marked with an asterisk were obtained with NN2; all others are the results of NN1.

the absorption coefficient: the rms error in μ_s' is 2.6%, whereas the rms error in μ_a is 14%. These are comparable with the errors observed in the training of the neural network.

In Table 3 we show the values of μ_a and μ_s' obtained from measurements at five different locations on one sample of bovine muscle. Both networks were used to analyze the data, and the differences in the estimates obtained with the two networks do not exceed the training errors. The rms variation among different locations was 16% in μ_a and 9% in μ_s'.

Examples of the diffuse reflectance measured for different tissues at 633 nm are shown in Fig. 7. Data for liver tissue were analyzed with NN2; for all other tissues NN1 was used. The results for 633

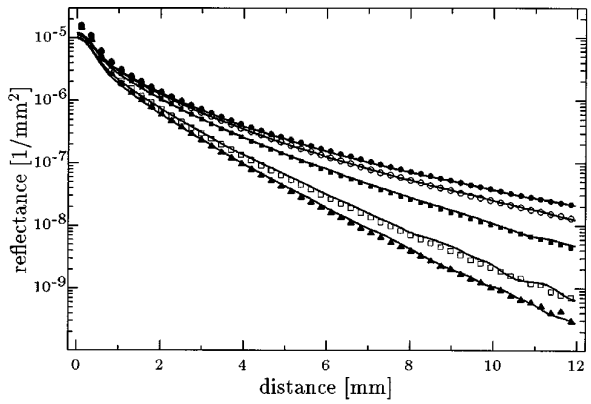

Fig. 6. Comparison of experimental measurements of spatially resolved diffuse reflectance (symbols) for five phantoms to Monte Carlo simulations (solid curves) generated with the true values of μ_a and μ_s'. The Monte Carlo simulations were obtained for pencil beams and convolved with the measured incident-beam profile. The optical properties for the five phantoms were μ_s' = 0.98, μ_a = 0.0033 (top curve); μ_s' = 0.98, μ_a = 0.0088; μ_s' = 0.97, μ_a = 0.025; μ_s' = 0.94, μ_a = 0.070; μ_s' = 0.93, μ_a = 0.100 mm^{-1} (bottom curve). Note that no parameter was fit.

Table 3. Optical Properties of Bovine Muscle at 633 nm Derived from Diffuse Reflectance Measurements at Five Different Locations on the Same Sample

	Neural Network 1		Neural Network 2	
Location	μ_a (mm^{-1})	μ_s' (mm^{-1})	μ_a (mm^{-1})	μ_s' (mm^{-1})
1	0.076	0.55	0.075	0.54
2	0.10	0.60	0.10	0.61
3	0.12	0.54	0.11	0.53
4	0.12	0.47	0.11	0.48
5	0.082	0.48	0.090	0.45

and 751 nm are presented in Table 4, in which the standard deviations were derived from measurements made at different locations on the same sample. These data are consistent with general findings in Ref. 5, namely:

(1) Although the reduced scattering coefficient varies by a factor of 3 from one tissue to another, the absorption coefficient can be different by 2 orders of magnitude. This reflects the difference in concentration of various chromophores such as hemoglobin.

(2) The reduced scattering coefficient is lower at 751 nm than at 633 nm for all tissue samples measured.

(3) Tissues with a higher hemoglobin content (bovine muscle and liver) show a larger decrease in μ_a at 751 nm compared with 633 nm than do less perfused tissues (adipose, chicken muscle).

As shown in Table 4, the only marked discrepancy between our results and published data is for μ_a in chicken muscle, which we found to be 3–4 times lower than that reported in other studies.

In the analysis above, the neural networks were trained with only the data beyond 2 mm from the source. In Fig. 6 we showed that good agreement between Monte Carlo simulations and experimental measurements could be obtained over the complete distance range for tissue-simulating phantoms. This was not the case for tissues, however. Initially

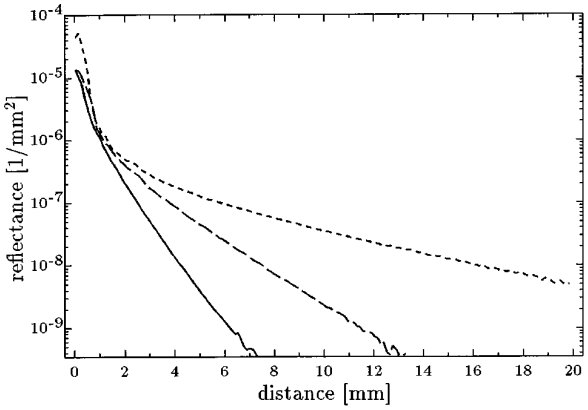

Fig. 7. Spatially resolved diffuse reflectance measured for chicken breast (short-dashed curve), bovine muscle (long-dashed curve) and bovine liver (solid curve) *ex vivo* at 633 nm. No polarizers were used.

Table 4. Optical Properties of Different Tissues *Ex Vivo* at 633 and 751 nm Derived by the Neural Networks from Spatially Resolved Absolute Diffuse Reflectance Measurements[a]

	λ = 633 nm		λ = 751 nm	
Sample	μ_a (mm^{-1})	μ_s' (mm^{-1})	μ_a (mm^{-1})	μ_s' (mm^{-1})
Bovine muscle	0.096 ± 0.015 (0.04–0.17)	0.53 ± 0.05 (0.44–0.70)	0.037 ± 0.007	0.34 ± 0.03
Bovine fat	0.0026 ± 0.0007	1.20 ± 0.07	0.0021 ± 0.0006	1.00 ± 0.05
Chicken breast	0.0038 ± 0.0008 (0.012–0.017)	0.42 ± 0.05 (0.33–0.80)	0.0027 ± 0.0010	0.28 ± 0.03
Bovine liver	0.30 ± 0.01 (0.27–0.32)	1.01 ± 0.08 (0.52–1.7)	0.17 ± 0.01	0.32 ± 0.02

[a]The standard deviation was calculated from multiple measurements at different locations on each sample. The values in parentheses are the ranges reported in Ref. 5.

we believed that this was due to the detection of light that was directly reflected from the relatively rough tissue surface. We attempted to exclude this light by polarizing the incident light and acquiring the CCD image through a crossed polarizer because the directly reflected light does not change its polarization. However, with these measurements, not only the directly reflected light but also light that has been remitted but not completely depolarized by the scattering processes is excluded. Thus the theoretical data for the Monte Carlo simulations, which were calculated for unpolarized light, should lie between the experimental curves measured with crossed and perpendicularly oriented polarizers. If the difference of the experimental curves is caused mainly by the directly reflected light, the theoretical curve of the Monte Carlo simulation should be close to the measurement with crossed polarizers.

In some cases the use of the crossed polarizers resulted in a data set that could be matched to a Monte Carlo simulation over the full distance range. For example, in Fig. 8(a) data for bovine fat obtained by the use of parallel and crossed polarizers are compared with the results of a Monte Carlo simulation generated with optical coefficients determined from the neural network. In contrast, a similar comparison for bovine muscle [Fig. 8(b)] shows that a good fit could not be achieved for distances of less than 2 mm, even when crossed polarizers were used. If the main reason for the difference between the experiments with crossed and parallel polarizers is due to light scattered from the surface, one might expect the effect to be reduced for a larger angle of incidence. However, Fig. 9 shows that, even for an angle of incidence of 45%, the difference between parallel and cross-polarization results persists for bovine muscle. Because of the failure of the model to predict accurately and consistently the reflectance close to the source, these data were not included in the analysis.

5. Discussion and Conclusions

Building on earlier work in video reflectometry,[13–17] we have described a different approach for acquiring and analyzing spatially resolved diffuse reflectance data from which estimates of the optical properties of tissues can be made. The novel features of the method are

(1) Absolute reflectance data are acquired when the reflectance images are referenced to images of

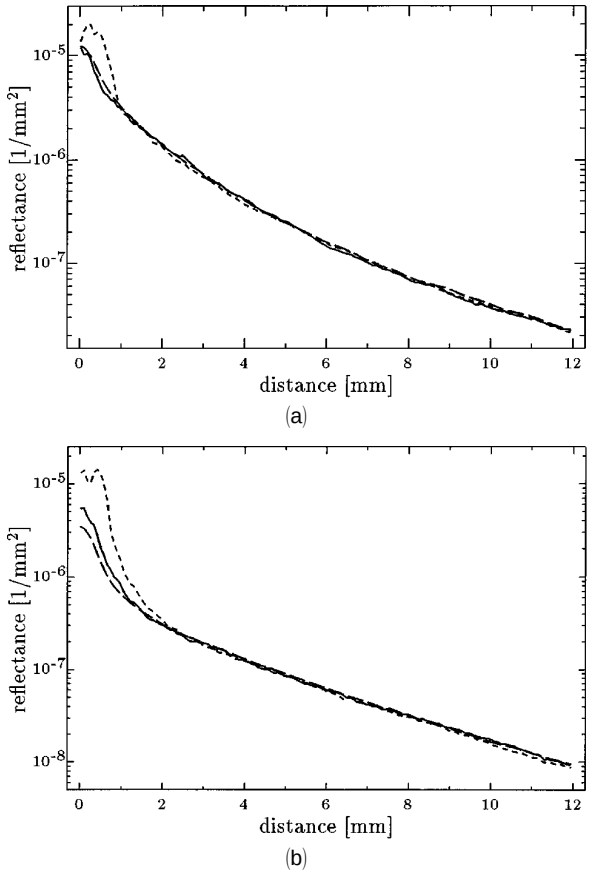

Fig. 8. (a) Spatially resolved diffuse reflectance measured for bovine adipose tissue at 751 nm with the detector polarizer parallel to the source polarizer (short-dashed curve) and with crossed polarizers (long-dashed curve). The solid curve is the result of a Monte Carlo simulation generated with the optical coefficients from the neural network with $g = 0.9$. Good agreement between the simulation and the result for crossed polarizers was obtained over the complete distance range. (b) Data obtained as above for bovine muscle at 751 nm. The Monte Carlo simulation agrees well beyond 2 mm, but closer to the source, even the data for crossed polarizers does not match the simulation.

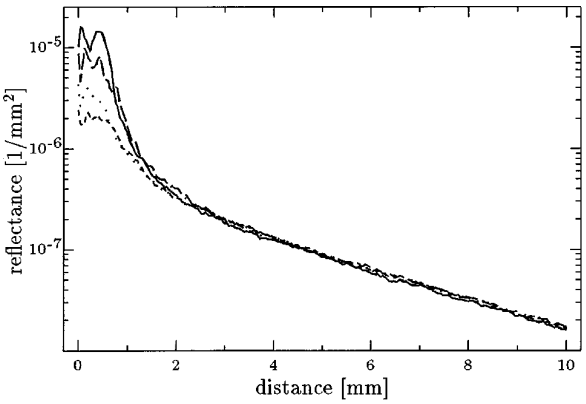

Fig. 9. Spatially resolved diffuse reflectance for bovine muscle at 751 nm. Measurements were made with the beam incident at 10° with parallel (solid curve) and crossed (dotted curve) polarizers and at 45° with parallel (long-dashed curve) and crossed (short-dashed curve) polarizers.

the incident beam. Other investigators have relied on relative reflectance data[12,13] or have made an auxiliary measurement of the total diffuse reflectance relative to a standard.[15]

(2) A neural network is used to extract the optical properties from the reflectance data. The network was trained with data from Monte Carlo simulations so, in this sense, an exact implementation of the radiation transport equation is used rather than an approximate model. To our knowledge, this is the first time a neural network trained with data from Monte Carlo simulations had been used for determination of the optical properties with reflectance measurements. When the neural network is used, the computation time needed for determination of the optical coefficients can be reduced by several orders of magnitude compared with that for a conventional fit routine. The neural network could also be trained with experimental data if materials with an appropriate range of known optical properties were available.

Regarding the first point, it is possible to train a neural network to use relative reflectance data (i.e., only the shape of the reflectance versus distance curve), and we have done this for a surface probe that mimics a matched boundary.[12] In the case of a mismatched boundary, however, we found that the training errors for μ_t' and μ_{eff} were ~12%, compared with 4% reported above for absolute reflectance data. Recalling that the rms errors associated with phantoms were ~2.6% in μ_s' and 14% in μ_a for absolute data, we conclude that the uncertainty for relative measurements would be ~3 times larger and too high for many applications. As in the case of matched boundary conditions, this might be improved if points closer to the source were included. We found, however, that, for real tissues, transport theory that did not include polarization-dependent scattering did not always provide an accurate description of the reflectance close to the source, even when crossed polarizers were used.

In this study we have used a mirror to reflect the incident beam into the camera so that it may be characterized for the measurement of absolute reflectance. An alternative approach would be to measure the spatially resolved reflectance for a material with known optical properties. As long as the source characteristics remain unchanged, data obtained for unknown materials could then be referenced to these data at each distance. Training the neural network on these ratios would be equivalent to using absolute reflectance values.

We also demonstrated in this paper that diffusion theory does not provide a sufficiently accurate calculation of the absolute diffuse reflectance at distances between 2 and 12 mm from the source if the refractive index is not the same inside and outside the turbid medium. Again this is in contrast to our previous experience with a matched surface probe,[12] in which diffusion theory was adequate at distances greater than one transport mean-free path from the source. This is also contrary to the experience of Jacques *et al.*,[15] who used diffusion theory to analyze their measurements of spatially resolved as well as total diffuse reflectance. Their analysis differed in that Eq. (1) was also integrated over ρ to provide an expression for the total diffuse reflectance. Because a separate measurement of total diffuse reflectance was made, this additional information was used to restrict the search for μ_a, μ_s' to those combinations that yielded the correct total diffuse reflectance. The combination chosen was that which gave the best agreement between Eq. (1) and the spatially resolved data. Jacques *et al.*[15] did not state specifically what distance range was used in their fitting, but they did not include "data too close to the point source." Measurements were made on only three phantoms, and rms errors of 3.6% in μ_a and 7.4% in μ_s' were reported, compared with our rms errors (on a larger data set) of 13.6% in μ_a and 2.6% in μ_s'. It is interesting to note that Jacques *et al.*[15] report larger errors in μ_s' than in μ_a, whereas the opposite was found in our study. A more complete comparison would be necessary to determine if this is characteristic of the two different methods. We assume that the separate measurement of the total diffuse reflectance by Jacques *et al.*[15] must contribute substantially to the accuracy of their results because, as shown above, reliance on the spatially resolved reflectance at some distance from the source as calculated by diffusion theory yields poor results.

Because our method does not rely on diffusion theory, in principle it can be applied to any combination of μ_s' and μ_a, although we have tested it only over the range $0.5 < \mu_s' < 2.5\ \text{mm}^{-1}$ and $0.002 < \mu_s' < 0.1\ \text{mm}^{-1}$. Of course, there would be practical problems associated with reflectance measurements on highly absorbing tissues.

Reasons for the disagreement between the theoreti-

cal values and the tissue experiments at small distances (i.e., less than 2 mm) from the incident beam could be

(1) In the Monte Carlo simulations we assume that $g = 0.9$. If the anisotropy parameter is smaller than this value, the reflectance at small distances is greater (see Fig. 4) and therefore the theoretical curves are closer to the experimental data.

(2) Because the disagreement is greater for muscle than for fat, there might be light piping effects in the fibers of the muscle that are not described by the simulations.

(3) The assumption of the Lambertian distribution causes an underestimation of $R(\rho)$ at small ρ (see Fig. 3).

We are currently investigating a number of improvements that would expand the potential of this technique. Although data close to the source were not used in the analysis, saturation of the pixels that correspond to these positions causes blooming in the detector and limits the exposure time. It should be possible to mask the CCD detector to avoid this problem. Simultaneous multiwavelength measurements could also be made by using a white-light source and a combination of beam splitters and filters in the detector optics. We have also begun to extend the analysis to layered tissues, although preliminary studies[28] indicate that additional information, such as layer thickness, must be known before reasonable estimates can be made of the optical properties of the different layers.

The method we have described avoids many of the problems inherent in contact-probe measurements. Because a full two-dimensional map of reflectance is obtained, future studies will be aimed at assessing the heterogeneity of real tissues and the impact of such heterogeneity on the estimation of average absorption and scattering coefficients.

This research was supported by the National Cancer Institute of Canada. Alwin Kienle is grateful for a doctoral scholarship from the German Academic Exchange Service.

References

1. M. S. Patterson, B. C. Wilson, and D. R. Wyman, "The propagation of optical radiation in tissue. 1. Models of radiation transport and their application," Lasers Med. Sci. **6,** 155–168 (1991).
2. M. S. Patterson, B. C. Wilson, and D. R. Wyman, "The propagation of optical radiation in tissue. 2. Optical properties of tissues and resulting fluence distributions," Lasers Med. Sci. **6,** 379–390 (1991).
3. A. Ishimaru, *Wave Propagation and Scattering in Random Media* (Academic, New York, 1978), Chaps. 7 and 9.
4. B. C. Wilson, "Measurement of tissue optical properties: methods and theory," in *Optical-Thermal Response of Laser-Irradiated Tissue,* A. J. Welch, and M. J. C. van Gemert, eds. (Plenum, New York, 1995), pp. 233–274.
5. W. Cheong, S. A. Prahl, and A. J. Welch, "A review of the optical properties of biological tissues," IEEE J. Quantum Electron. **26,** 2166–2185 (1990).
6. J. W. Pickering, S. A. Prahl, N. van Wieringen, J. F. Beek, H. J. C. M. Sterenborg, and M. J. C. van Gemert, "Double-integrating-sphere system for measuring the optical properties of tissue," Appl. Opt. **32,** 399–410 (1993).
7. A. Kienle, R. Hibst, and R. Steiner, "The use of a neural network and Monte Carlo simulations to determine the optical coefficients with spatially resolved transmittance measurements," in *Laser-Tissue Interaction V,* S. L. Jacques, ed., Proc. SPIE **2134,** 364–371 (1994).
8. L. Lilge, T. How, and B. C. Wilson, "Miniature isotropic optical fibre probes for quantitative light dosimetry in tissue," Phys. Med. Biol. **38,** 215–230 (1993).
9. M. S. Patterson, B. Chance, and B. C. Wilson, "Time resolved reflectance and transmittance for the noninvasive measurement of tissue optical properties," Appl. Opt. **28,** 2331–2336 (1989).
10. M. S. Patterson, J. D. Moulton, B. C. Wilson, K. W. Berndt, and J. R. Lakowicz, "Frequency-domain reflectance for determination of the scattering and absorption properties of tissue," Appl. Opt. **30,** 4474–4476 (1991).
11. G. Yoon, D. N. Ghosh Roy, and R. C. Straight, "Coherent backscattering in biological media: measurement and estimation of optical properties," Appl. Opt. **32,** 580–585 (1993).
12. T. J. Farrell, M. S. Patterson, and B. C. Wilson, "A diffusion theory model of spatially resolved, steady-state diffuse reflectance for the noninvasive determination of tissue optical properties *in vivo,*" Med. Phys. **19,** 879–888 (1992).
13. R. A. Bolt and J. J. ten Bosch, "Method for measuring position-dependent volume reflection," Appl. Opt. **32,** 4641–4645 (1993).
14. R. A. Bolt and J. J. ten Bosch, "On the determination of optical parameters for turbid materials," Waves Random Media **4,** 233–242 (1994).
15. S. L. Jacques, A. Gutsche, J. Schwartz, L. Wang, and F. K. Tittel, "Video reflectometry to extract optical properties of tissue *in vivo,*" in *Medical Optical Tomography: Functional Imaging and Monitoring,* G. Mueller, B. Chance, R. R. Alfano, S. R. Arridge, J. Beuthan, E. Gratton, M. Kaschke, B. R. Masters, S. Svanberg, and P. van der Zee, Vol. ISII of SPIE Institute Series (Society of Photo-Optical Instrumentation Engineers, Bellingham, Wash., 1993), pp. 211–226.
16. R. Splinter, G. A. Nanney, L. Littmann, C. H. Chuang, R. H. Svenson, J. R. Tuntelder, and G. P. Tatsis, "Monitoring tissue optical characteristics *in situ* using a CCD camera," Laser Life Sci. **6,** 15–25 (1994).
17. M. Dogariu and T. Asakura, "Reflectance properties of finite-size turbid media," Waves Random Media **4,** 429–439 (1994).
18. A. Kienle, "Lichtausbreitung in biologischem Gewebe," Ph.D dissertation (University of Ulm, Germany, 1994).
19. T. J. Farrell, B. C. Wilson, and M. S. Patterson, "The use of a neural network to determine tissue optical properties from spatially resolved diffuse reflectance measurements," Phys. Med. Biol. **37,** 2281–2286 (1992).
20. B. C. Wilson and G. Adam, "A Monte Carlo model for the absorption and flux distribution of light in tissue," Med. Phys. **10,** 824–830 (1983).
21. L. Wang and S. L. Jacques, *Monte Carlo Modeling of Light Transport in Multi-Layered Tissues in Standard C* (Anderson Cancer Center, University of Texas M. P. Anderson Cancer Center, Houston, Texas, 1992).
22. F. P. Bolin, L. E. Preuss, R. C. Taylor, and R. J. Ference, "Refractive index of some mammalian tissue using a fiber optic cladding method," Appl. Opt. **28,** 2297–2303 (1989).
23. L. G. Henyey and J. L. Greenstein, "Diffuse radiation in galaxy," Astrophys. J. **93,** 70–83 (1941).
24. L. R. Poole, D. D. Venable, and J. W. Cambell, "Semianalytic Monte Carlo radiative transfer model for oceanographic lidar systems," Appl. Opt. **20,** 3653–3656 (1981).

25. D. R. Wyman, M. S. Patterson, and B. C. Wilson, "Similarity relations for anisotropic scattering in Monte Carlo simulations of deeply penetrating neutral particles," J. Comput. Phys. **81,** 137–150 (1989).
26. B. C. Wilson, M. S. Patterson, and B. W. Pogue, "Instrumentation for *in vivo* tissue spectroscopy and imaging," in *Medical Lasers and Systems II,* D. M. Harris, C. M. Penney, and A. Katzir, eds., Proc. SPIE **1892,** 132–147 (1993).
27. J. B. Fishkin, P. T. C. So, A. E. Cerussi, S. Fantini, M. A. Franceschini, and E. Gratton, "Frequency-domain method for measuring spectral properties in multiple-scattering media: methemoglobin absorption spectrum in a tissuelike phantom," Appl. Opt. **34,** 1143–1155 (1995).
28. A. Kienle, L. Lilge, M. S. Paterson, B. C. Wilson, R. Hibst, and R. Steiner, "Investigation of multi-layered tissue with *in vivo* reflectance measurements," in *Photon Transport in Highly Scattering Tissue,* S. Avrillier, B. Chance, G. J. Mueller, A. V. Priezzhev, and V. V. Tuchin, eds., Proc. SPIE **2326,** 212–221 (1994).